Final Draft
of the original manuscript:

Staneva, J.; Stanev, E.V.; Wolff, J.-O.; Baldewien, T.H.; Reuter, R.;
Flemming, B.; Bartholomae, A.; Bolding, K.:

Hydrodynamics and sediment dynamics in the German Bight. A focus on observations and numerical modelling in the East Frisian Wadden Sea

In: Continental Shelf Research (2008) Elsevier

DOI: 10.1016/j.csr.2008.01.006

Hydroynamics and Sediment Dynamics in the German Bight. A Focus on Observations and Numerical Modelling in the East Frisian Wadden Sea.

Joanna Staneva [a,1,*], Emil Stanev [b,1], Jörg-Olaf Wolff [a], Thomas H. Badewien [c], Rainer Reuter [c], Burghard Flemming [d], Alexander Bartholomä [d], Karsten Bolding [e]

[a] *Institute for Chemistry and Biology of the Sea (ICBM), University of Oldenburg, Carl-von-Ossietzky-Strasse 9-11, D-26111 Oldenburg, Germany*

[b] *School of Environmental Science, University of Ulster, Cromore Road, Coleraine, BT52 1SA, UK*

[c] *Institute of Physics, University of Oldenburg, Carl-von-Ossietzky-Strasse 9-11, D-26111 Oldenburg, Germany*

[d] *Senckenberg Institute, Department for Marine Science, Südstrand 40, D-26382 Wilhelmshaven, Germany*

[e] *Bolding and Burchard Hydrodynamics, Strandgyden 25, DK-5466 Asperup, Denmark*

Abstract

This work deals with analysis of hydrographic observations and results of numerical simulations. The data base includes ADCP observations, continuous measurements on data stations and satellite data originating from the Medium Resolution Imaging Spectrometer (MERIS) onboard the ESA satellite ENVISAT with a spatial resolution of 300 m. Numerical simulations use nested models with horizontal resolutions ranging from 1 km in the German Bight to 200 m in the East Frisian Wadden Sea coupled with a suspended matter transport model. Modern satellite observations have now a comparable horizontal resolution with high-resolution numerical model of the entire area of the East Frisian Wadden Sea allowing to describe and validate new and so far unknown patterns of sediment distribution. The two data sets are consistent and reveal an oscillatory behavior of sediment pools to the north of the back-barrier basins and clear propagation patterns of tidally driven suspended particulate matter outflow into the North Sea. The good agreement between observations and simulations is convincing evidence that the model simulates the basic dynamics and sediment transport processes, which motivates its further use in hindcasting, as well as in the initial steps towards forecasting circulation and sediment dynamics in the coastal zone.

Preprint submitted to Elsevier *9 January 2008*

Key words: Ocean circulation, Sediment Dynamics, Tidal Basins, Nested Models

1 Introduction

Near-coastal areas are subject to increasing practical and societal interests, however our basic scientific knowledge is still limited and forecasting capabilities are still in their infancy. One of the basic problems is the insufficient resolution of observations and models in the near coastal zone, which necessitates further efforts towards downscaling. When approaching the coast the overall role of bottom turbulence and sediment dynamics increases, the latter controlling coupling between water-, ecosystem- and morphodynamics. Resolving the coastal boundary layer requires further synergy between newly available data characterized by fine resolution in time and space and modelling with very fine resolution. In this paper we describe the downscaling from a regional model for the area of the German Bight to a model for the East-Frisian Wadden Sea. The work presented here has been carried out within the framework of the research programme "BioGeoChemistry of Tidal Flats", where observations based on data from in-situ instrumentation, e.g. temperature, salinity sensors and Acoustic Doppler Current Profilers (ADCP), as well as ocean colour sensors onboard satellites, were combined with theoretical studies and numerical modelling. The major aim of this research is: (1) to make a decisive step towards downscaling, (2) to understand dynamic processes in the German Bight and the Wadden Sea, (3) to develop techniques making the best use of data coming online in the near future, and (4) to extend the analysis of data and simulations of earlier studies over longer periods. All these are new aspects of studies in the area of interest, which have not been addressed in the earlier studies. The results presented here are relevant to other similar cases of coastal dynamics, thus having wider application beyond the current studied area.

The German Bight (Fig. 1a), which is bordered by the coasts of the Netherlands, Germany and Denmark, is situated in the south-eastern corner of the North Sea. The East-Frisian Wadden Sea is one of the shallowest areas of the German Bight, being characterised by a series of barrier islands, each 5-10 km long in the east-west direction and 2-3 km wide (Fig. 1b). The tidal signal associated with the amphidromy at $\sim 55.5°$ N, $\sim 5.5°$E travels along the northern boundary of the area (Fig. 1b) in $\sim$ 50 minutes. The tidal range

* Corresponding author.
Email address: Joanna.Staneva@gkss.de (Joanna Staneva).
[1] Present address: Institute for Coastal Research, GKSS Research Center, Max-Planck-Strasse 1 D-21502 Geesthacht, Germany

varies from $\sim$ 2.5 m (Islands Borkum and Sylt) to $\sim$ 3.5 m (the Elbe river mouth), i.e., the region is exposed to upper mesotidal conditions. The volume of water exchanged between the North Sea and an individual tidal basin during a tidal cycle is much higher than the volume of water which resides in the basin under low water conditions. In similar settings, the transports through the inlets have different characteristic times during ebb and flood (Stanev et al., 2003a,b).

The Wadden Sea is a highly dynamic tidal area where the conditions in the water column vary widely with season, tide and meteorological conditions. A fundamental characteristic of this area is the vigorous suspended matter dynamics. For example, up to 7200 tons of mud and 4300 tons of sand are transported in and out of the tidal channel of the Otzumer Balje (Fig. 1b) over one tidal cycle (Santamarina Cuneo and Flemming, 2000). The water, especially in the back-barrier tidal flats, is characterised by high loads of suspended matter, which often reached concentrations of about 100 mg/l. Typical Secchi depths in this shallow area are 0.1 to 0.5 m, depending on water depth, tidal current speed, suspended material, and wind.

Traditionally, data for the Wadden Sea originate from ship surveys, tide gauges and other time series stations. Earlier observations were not able to resolve the complex dynamics spatially, and information on horizontal patterns in particular suspended sediment transport, was usually provided by numerical models (Puls and Sundermann, 1990, Pleskaschevski et al., 1995, Gayer and Dick, 2006, Stanev et al., 2007a,b and the references therein). Obviously, a detailed validation of numerical models against observations is needed not only at fixed locations, as done by Stanev et al. (2003a; 2007b), but also over larger areas in order to objectively assess the level of realism of the current simulations.

For the open ocean, a ground resolution of about one kilometer might be sufficient for validation of the basic model dynamics. Such resolution is currently provided by ocean colour sensors such as MODIS and SeaWiFS, which have a spatial resolution of 1000 m and 1100 m, respectively. However, a resolution of about 1 km is not sufficiently fine in the near coastal zone where the scales determined by local topography and contrasting dynamics are much smaller. It appears that, for such areas, satellite images with the capability of resolving small-scale structures well below 1 km have to be used. Such resolution is currently provided by the MEdium Resolution Imaging Spectrometer (MERIS) onboard the ESA satellite ENVISAT. The validation of the simulated dynamics and sediment dynamics is a major research interest here. The usefulness of combining remote sensing and numerical modelling when studying oceanographic processes in the German Bight with a focus on the East Frisian Wadden Sea is demonstrated in this paper. It is structured as follows: the observational data are described in Section 2, followed by a description of

the models and the results of our simulations in Section 3. The validation of the model is presented in Section 4, followed by brief conclusions.

2 Observations

The German Bight has in recent years been the subject of detailed national and international investigations (see e.g. Droppert et al., 2000 Becker et al., 1999). It is well established that the wind in this area of the North Sea results in a cyclonic residual circulation, i.e. a circulation in the direction of propagation of the tidal wave (from west to east along the southern boundary and from south to north along the coasts of Germany and Denmark). Under the dominating influence of tides, wind, and wind waves a specific coastal water mass is formed, which is rich in nutrients and suspended particulate matter, thereby supporting a diverse flora and fauna. This water mass is periodically exposed to mixing with North Sea waters (during flood), and is partially exported back into the North Sea (during ebb). In this way the Wadden Sea acts as a buffer zone between ocean and land. However, neither the interaction between the North Sea and the German Bight, nor the exchange of water and properties between the Wadden Sea and the German Bight are quantitatively known. This is partially due to the limitation of present-day observations and hence an insufficient availability of data for numerical modelling. The application of observations carried out within the framework of the research programme "BioGeoChemistry of Tidal Flats" (WATT) for the purpose of advancing our understanding of German Bight-Wadden Sea dynamics and sediment dynamics is illustrated in the present paper.

2.1 Observations at the WATT-Data Station

A time-series station was erected in the Otzumer Balje, i.e. the tidal inlet between the islands of Spiekeroog and Langeroog (see e.g. Reuter, 2005). The station is located at 53°45'01" N, 7°40'16" E. Charted water depth (below mean low water at spring tide) is 11.5 m. Technical characteristics, including information about measured parameters and data types are given in Appendix 1.

The observed air and sea surface temperatures are dominated by a clear seasonal cycle with a range of about 20°C (Fig. 2a). No clear difference between atmospheric temperature and Sea Surface Temperature (SST) is observed on the seasonal scale. This is just an illustration for the very small heat capacity of the Wadden Sea, unlike the situation in the deep ocean. On a synoptic interval (one week) the range of air temperatures is several times higher than

that of the SST.

The seasonal and interannual variations in salinity are less periodic than those of temperature and are much more difficult to explain, partially because the correlation with fresh water fluxes is less obvious than for some other ocean areas. It is trivial to expect that the temporal variability of surface salinity (Fig. 2b) should reflect the dilution on the tidal flats by direct precipitation and run-off from land (eventually including sub-terrainian waters). However, the situation is made more complicated by human-controlled fresh water release from lakes, which serving as buffers for excess fresh water on land.

The positive correlation between salinity and sea level (Fig. 3) is easy to establish from the observations on the data station. This positive correlation is due to the fact that before high water the transport through the inlet is directed from the open ocean (high salinity) to the tidal flats. The sharp decrease in salinity resulting from the release of fresh water from a coastal lake, is followed by an increase in the range of salinity oscillations (indicative of stronger mixing between open and coastal ocean), which then constantly (exponentially) decreases before the next release of fresh water.

In recent years, ADCP data have been widely used in oceanography and contributed substantially to the understanding of the basic dynamics of the coastal ocean (Valle-Levinson and Lwiza, 1995; Münchow, 1998). The validation of the numerical model, which is the central topic of this paper, has largely benefited from recent data measured with an upward-looking ADCP (Fig. 4). In this paper is illustrated one sub-sample of this data series in order to present its quality and to discuss some aspects of the circulation: Fig. 4 displays current speed; Fig. 5 presents the temporal evolution of horizontal velocity (upper two panels) and vertical change in horizontal velocity (bottom panel). The starting time of both figures is 16.03.2005.

The observations provide high-quality signals which allow addressing the temporal variability of velocity profiles over long time spans. This is an advancement in comparison with the study of Stanev et al. (2003a and 2007b) addressing current variability over a few tidal periods only.

However, the velocity profiles do not sufficiently resolve the frictional dependence of velocity in the bottom layer, i. e. the well known logarithmic profile (the violet areas marking low current speeds do not reach the bottom of the plot at all times), because the sensor is located at 70 cm above the bottom. Nevertheless, it is clear from Fig. 4 (bottom panel) and Fig. 5 (bottom panel) that larger velocity shear is observed during ebb (during this time the velocity is higher, as well).

The temporal characteristics of the dynamics in tidal inlets are well captured by the ADCP, which partially supports the results of Stanev et al. (2003a)

and shows that the maximum ebb velocity slightly exceeds the maximum flood velocity. In the above study, a major asymmetry was revealed by the longer time $T_{e\rightarrow f}$ needed for the transition between maximum ebb and maximum flood as compared to the time needed for the inverse transition $T_{f\rightarrow e}$ ($T_{e\rightarrow f} : T_{f\rightarrow e} = 2 : 1$). This is called "shorter-falling" asymmetry (in the terminology of Friedrichs and Madsen, 1992). A similar asymmetry is observed in the present data displaying the hypsometric control (Stanev et al., 2003a). However, the results of the two studies are not identical because Stanev et al. (2003a) addressed observations across sections, whereas here only local observations have been adressed. In the present observations one clearly notices the missing balance between locally measured inflowing and outflowing water (more export than import), which was not the case in Stanev et al. (2003a) where the integrated cross-channel transport was much better balanced. However, the present results seem to support the results of Stanev et al. (2007b) by indicating that the left bank (looking in the direction of the North Sea) is an ebb-dominated area (not only because of the pure temporal asymmetry but also because the ebb velocities are higher). In earlier ADCP observations it was already noticed that the flood flow (Fig. 4) reaches maximum speeds at the sea surface, whereas this is not the case for the ebb flow. More detailed examination of data for other periods reveals similar reverse "asymmetries" (surface maximum during ebb and reverse during flood), this signature of the surface transport being induced by wind opposing one of the two currents (depending on whether the wind blows in the direction of the flow or in the opposite direction).

The results displayed in Fig. 5 convincingly demonstrate the large non-tidal variability of the current, observed as the difference between the speeds of two consecutive M2 periods ($v(t + \delta t) - v(t)$, where δt =24 h 50 min, i.e. a lag of 149 5-min data). The signal in the upper panel of Fig. 5 does not present any clear periodicity. Shortening the offset to 30 minutes reveals that the maximum acceleration of current occurs almost immediately after high and low water. This acceleration period increases substantially during neap tides, in particular during the flood phases, which is consistent with the earlier observations analysed by Stanev et al. (2007a).

The ADCP data resolve the vertical shear velocity of the horizontal velocity in most of the water column very well, as represented in the bottom panel of Fig. 5 by the difference between the current speeds at every two depths displaced by 4 m (this value is choosen because smaller distances result in larger noise levels). It is obvious that the largest shears occur in the surface mixed layer (about 1 m thick) because of the difference in wind and current directions. Positive or negative velocity shear can be observed either during the ebb or the flood phase, simply depending on the direction and speed of the wind. The maximum velocity shear is clearly observed throughout the entire water column, particularly during the ebb tide. It is challenging to try (as

shown below) to check the consistency between "abundant" different current structures observed at the data station and in the numerical simulations.

2.2 Ocean Colour Imagery in Turbid Coastal Waters

The observation of ocean colour in coastal zones from satellites facilitates the understanding of important hydrodynamic and sediment processes. Because resolving the different water constituents in tidal flat regions such as the Wadden Sea is of prime interest, there is a need to use multispectral measurements (Gemein et al., 2006). However, most of the operating satellite sensors neither resolve the processes well in space, nor have sufficient spectral resolution. Compared with earlier sensors, MERIS, with its many spectral bands especially in the Near InfraRed (NIR), gives good accuracy for water constituent determinations (compared to SPOT and LANDSAT, Doxaran et al., 2004, Lehner et al., 2004), which are not specialised for water constituents). The only sensor that comes close to MERIS is OCM. It has a spatial resolution of 350 m and a global coverage of two days with eight bands and 20 nm bandwidth for the first six bands (Sarangi et al., 2001).

MERIS is a hyperspectral sensor with a ground resolution of 300 m for full resolution images. The spectrometers create a bi-dimensional image on the Color-Capture Devise (CCD, ESA, 2003). One dimension is the spatial extension; the other is the spectrum, from 390 to to 1040 nm in 15 programmable bands (ESA, 2004). The revisiting time of ENVISAT is two days for latitudes north of 50° (Doerfer et al., 1999). Around 53°43'N and 7°30'E, which is the area of interest, one image is available every second day. The data processing is addressed in detail by Gemein et al. (2006), where more than 90 usable images of the research area have been analysed between June 2002 and April 2005. The output consists of the concentrations of chlorophyll-a (CHL), total suspended matter (TSM), and the absorption coefficient of yellow substance (YS) at 412 nm. For the validation of MERIS-derived suspended matter concentrations in the Wadden Sea, filtration data of ship cruises from 2003 to 2005 have been used (Gemein et al., 2006).

Two principally different suspended sediment regimes in the German Bight can be inferred from Fig. 6: high concentrations during the cold part of the year (air temperatures corresponding to Fig. 6a and Fig. 6c are 7°C and 4°C , respectively) and low concentrations in summer (air temperature 15°C corresponds to Fig. 6b). During winter, the sharp transition between back-barrier water and water of the German Bight breaks up, and the sediment patterns penetrate deeply into the German Bight (Fig. 6a and Fig. 6c). The analysis of a number of winter maps (not shown here) demonstrated that, although the wind speed is usually higher in this part of the year, the high suspended

sediment concentrations can not be explained solely by the wind impact. The explanation of the increased sediment concentration in winter necessitates considering the dependence of the settling velocity on the kinematic viscosity, the latter depending on temperature (Kroegel and Flemming, 1998; Flemming, 2004). As the settling velocities are smaller in winter the sediment remains longer in the water column, which results in a larger extension of areas with high concentrations. The largest measured concentration was 300 mg/l in the Spiekeroog inlet during ebb tide on 20 Jan 2004 (filtration data), with wind speeds of 5 to 15 m/s the days before.

Figure 6 demonstrates that the resolution of the MERIS sensor responds well to the needs of sediment studies in the German Bight. The horizontal patterns of Suspended Particulate Matter (SPM) are dominated by transport, which is documented by large sediment concentrations in front of the tidal inlets. These high concentrations are connected with sediment clouds originating from the tidal basins from where they propagate northwards. While some horizontal patterns observed in the MERIS data are already known from numerical simulations (Stanev et al., 2007a,b), the pattern shown in Fig. 6a seems to be new. This pattern is characterised by several filaments of high SPM concentration originating from the tidal channels and penetrating deeply into the German Bight. It seems that these filaments with high SPM concentration are not directly connected with the tidal fronts, a conclusion which is supported by the lack of correlation between these patterns and topography. A more plausible explanation is that these high-concentration zones display the fate of sediment clouds originating from the tidal basins, which later become subject to east-west tidal oscillations, the latter modulating the spatial properties of the SPM.

3 The Numerical Simulations

3.1 Model Set-up

Resolving ocean dynamics in ocean models for regions next to the coast means resolving the coastal boundary layer. This requires complex physics and very fine resolution. When approaching the coast, the importance of sediment dynamics increases because it becomes coupled with water and morphodynamics. In a recent study of Stanev et al. (2007a), it is demonstrated that the turbulent kinetic energy is one of the main drivers of the dynamics of suspended particulate matter. Its absolute maxima are observed in the tidal inlets and their funnel-like extensions. The minima are in the back-barrier area where they approximately coincide with the watersheds separating the individual basins. During most of the time, the entire water column shows a high level of tur-

bulence. Only during slack water (duration of about 1 hour) does the velocity reduce drastically and the level of turbulence diminish, which enables the deposition of sediment. Therefore, one important consideration when developing sediment transport models is to ensure correct prediction of turbulence, and adequate vertical resolution (see Appendix 2).

The model used here is a 3-D primitive equation numerical model (Burchard and Bolding, 2002), in which the equations for the three velocity components u, v and w and sea-surface height ζ, as well as the equations for turbulent kinetic energy (TKE) k and the eddy dissipation rate (EDR) ε due to viscosity are solved. The model is coupled with a sediment transport model, in which mud particles of a grain size of $d = 63\mu m$ are considered. The model uses a standard diffusion-advection equation for the concentration of suspended sediment. A short presentation of this model and some technical details are given in Appendix 2.

The application of the model to the area of our study is described by Stanev et al. 2007b - see this paper for more details). The model uses terrain-following equidistant vertical coordinates (σ-coordinates). The vertical column is discretized into ten non-intersecting layers.

The nested-grid model consists of three model configurations: a coarse-resolution North Sea-Baltic Sea (about 5 km) outer model, a fine-resolution (about 0.8 km) inner model covering the German Bight and a very fine-resolution (about 200 m) model for the Wadden Sea region resolving the barrier islands and the tidal flats. The horizontal discretization is done on a spherical grid. The bathymetric data for the different model configurations are prepared using the ETOPO-1 topography, together with observations made available from the German Hydrographic Service (Bundesamt für Seeschiffahrt und Hydrographie, BSH, Dick et al., 2001)

The model system is forced by: 1) atmospheric fluxes estimated by the bulk formulation using 6-hourly ECMWF re-analyses data from 1986 to 2005, 2) hourly river run-off data provided by the BSH operational model, and 3) time-varying lateral boundary conditions of sea surface elevations and salinity.

The sea surface elevations of the open boundary of the North Sea-Baltic Sea model are generated using tidal constituents obtained from the TOPEX/POSEIDON data. Temperature and salinity at the open boundary of the outer model are interpolated at each time step using the monthly mean climatological data of Janssen et al. (1999). In this study, the nesting is done one-way only, i.e., the nested models receive boundary values from the coarser model but do not influence the coarser resolution of the model. For more detail of the nested-grid models we refer to Staneva et al. (2007).

With a horizontal resolution of 200 m, the area in Fig. 1b is resolved with

$324x88$ grid-points in the zonal and meridional direction, respectively. The forcing at the open boundaries is taken from the simulations with the German Bight Model (GBM, Staneva et al., 2007). Although the Wadden Sea is a well-mixed water body (Stanev, 2007a), the correct prescription of fresh-water fluxes at the coast is necessary in order to enable an adequate simulation of water properties. The fresh-water fluxes from the main tributaries in the region are taken from the observations compiled in an internal report of the Niedersächsischer Landesbetrieb für Wasserwirtschaft und Küstenschutz, Aurich, Germany. The sea-level data at the Wadden Sea open boundaries have been taken from the model output provided by the GBM and interpolated in time and space onto the grid points along the boundaries of the Wadden Sea regional model. The lateral boundary conditions for concentration are taken to be zero for inflowing water. This assumption agrees with satellite data and direct observations and demonstrates that concentrations along the northern model boundary are small (at least five times smaller than in the tidal basins). Outflowing water results in a sediment flux $u_n c$ out of the model area, where u_n is the velocity normal to the boundary.

4 Numerically Simulated Circulation. The horizontal patterns

The present numerical simulations differ from earlier ones in the same area (Stanev et al. 2003a,b; 2007b) by: (1) focussing on the German Bight, (2) longer time integration, and (3) focus on the baroclinic circulation. In this section the major results will be illustrated using horizontal patterns of some simulated variables.

Figure 9 shows a time-average of the vertically integrated circulation for the German Bight for the six years period 2000-2005. In most of the German Bight area, the residual circulation is cyclonic due to the dominant eastward wind forcing. The circulation is more intensive off-shore and near the open boundaries of the German Bight. A local minimum of the circulation occurs in the coastal areas of the Bight and in the north-eastern part.

The importance of prescribing correct fresh water forcing becomes obvious from Fig. 8, which describes the horizontal surface salinity distribution for two particular cases during high water and low water on 05.03.2005 and 28.03.2005, correspondingly. The largest gradients are simulated in the areas of river mouths (Elbe, Weser and Ems). Protrusions of diluted waters are better seen during low water both deep in the German Bight, as well as over the tidal flats (water from Weser River into the tidal basins, or in case with eastward wind from Ems River into the tidal basins). The former can be considered as a coarse-resolution analogue of the protrusions observed in the sediment from MERIS satellites (Fig. 6b). This could be a model arte-

fact associated with insufficient resolution of the GBM in the Wadden Sea. Furthermore, it is clear that, although the situation in the German Bight correlates with existing concepts about salinity distribution, the simulations in the East Frisian Wadden Sea suffer from insufficient horizontal resolution of the model, in particular in the connecting inlets. The influence of the river run-off and and atmospheric forcing is clearly observed by the difference of the distribution of low salinity waters between the two horizontal patterns.

Analyses of the circulation simulated in the Wadden Sea has been previously reported by Stanev et al., (2003a and 2007a), mainly focusing on the tidal variability. However, in the previous studies, tidal forcing has been taken from the BSH operational model output, whereas in this paper the one-way nesting techniques that utilizes the GBM output to force the Wadden Sea model set-up is used. The present simulations (Fig. 9) are in overall consistency with the earlier ones, in particular as it concerns the transport through the straits, the situation in the region being very strongly dependent on the hypsometry of the tidal basins and tidal forcing (the latter being rather periodic). The general pattern is characterized by extreme velocities in the tidal inlets, westward currents in front of the barrier islands during ebb, and eastward currents during flood.

The salinity distribution (Fig. 10) reveals that the strong gradients simulated by the model are comparable with the observed values. They originate from the sluices at the coast, which are open during low water. With increasing sea level during flood, these waters are "pressed" along the coast. Furthermore, regions close to the deep channels are first filled with open-ocean water. The situation in the open sea (north of the barrier-islands) is characterized by high salinity values, which are much more uniform at high water than during low water. In the latter period, the structure of the salinity field (north of the barrier-islands) is geometrically similar, but inverse to that of suspended sediment concentration (Fig. 6a, b). The along-channel gradient of salinity of about 5 psu/10 km agrees well with the Lagrangean observations of Punken (personnal communications).

The horizontal patterns of suspended sediment in the Wadden Sea (Fig. 11) area reveal some differences, but also similarities with those of salinity distribution (compare with 10). These differences and similarities can be explained having in mind (1) the distributions of sources, and (2) the different impact of circulation and turbulence on salinity and SPM. As it concerns the source terms, the near coastal areas give the origin of low salinity and high SPM concentration, therefore during low water low salinity and high sediment concentration is observed north of the tidal inlets. However, in contrast to salinity, which has one maximum per tidal period in tidal channels, sediment concentration has two maxima, which is due to the role of turbulence (Stanev et al., 2007a) controlling the erosion and deposition processes.

The quantitative agreement between SPM simulations and observations based on MERIS data, which is discussed in more detail further in this paper (see also Gemein et al., 2006), gives some confidence to use the analysis of simulated SPM patterns in order to comment on some important processes. North of the back-barrier islands cloud-like shape zones of increased sediment concentrations are observed both during low and high water. These sediment clouds oscillate in east-west direction revealing clearly the so called tidal excursions. They reach their easternmost displacement during high water (Fig. 11a), during which time, the southern transport squeezes them close to the barrier islands. The migration of sediment clouds north of the barrier islands enables the SPM to leave one tidal basin and enter a neighbouring one via the open ocean (Stanev et al., 2007a).

5 Comparison of Numerical Simulations with Observations

Validation of numerical models in near-coastal areas is still a matter of ongoing research, and there are a number of problems to be solved before adequate agreement between simulations and observations can been reached. It is obvious from Fig. 4 and Fig. 3 that extremely complex dynamics and fresh water fluxes from land make the performance of coastal models problematical, mostly due to the inaccuracy of the forcing data.

Despite these mentioned problems, these simulations seem encouraging. It is not only the seasonal course of sea surface temperature in the German Bight (location - $54°7''$N $7°, 27''$ E), but also the surface-to-bottom difference in observations and simulations that agrees well (Fig. 12). This result is indirectly confirmed by the adequate simulation of the vertical salinity/density stratification. The horizontal patterns of salinity, which have been discussed in the previous section, give additional proof.

As far as the salinity of the WATT-data station is concerned, the agreement between simulations and observations is better than expected, in spite of possible problems with fresh water fluxes from land, (Fig. 13). However, this agreement between observations and simulations is not too surprising, considering the good model performance in reproducing transports (Fig. 14).

The validation of the simulations for the suspended sediment is based on direct observations and remote sensing data. Direct observations have been carried out by Jördel et al. (2004) in the Otzumer Balje (Fig. 1). Currents were recorded over the entire water column using an acoustic Doppler current profiler (ADCP). A laser in-situ scattering and transmissiometry (LISST) system was used to determine particle-size distributions of suspended sediments in the water column. In-situ measurements obtained by means of a flow-volume-

controlled pump centrifuge were used to calibrate the signal from the acoustic and optical instruments. As demonstrated in Fig. 15a, the phase of the signals from observations and numerical simulations agrees quite well and the amplitudes are comparable. Further support of this good agreement between our simulations and observations has been presented in Gemein et al. (2006) where satellite data with high spatial resolution have been compared with simulations. These remote sensing data are essentially the same as the ones shown in Fig. 7. In Fig. 15b we compare the mean SPM concentrations along transects parallel to the coast with data from a satellite image for a high-water scene to ensure water coverage for the whole area. The agreement between the mean cross-shore distribution of SPM in the model and the data is much better than one would expect from a model that has not been especially calibrated for this situation.

Because a general consistency between simulations and observations is searched in this paper, the mean concentrations along transects parallel to the coast are compared below. The chosen image is a high-water scene which ensures water coverage of the whole area. The (model) zonal mean SPM concentrations (Fig. 15b) reveal the main cross-shore distribution pattern of SPM. The agreement with the simulations are better than one would expect for a model which has not been well calibrated to replicate the observed features of SPM.

6 Conclusions

This study aims at improving the understanding of the circulation and sediment dynamics of the German Bight and the Wadden Sea using different data from observations and an up-to-date circulation model. The observational data base includes ADCP observations, laser in-situ scattering and transmissiometry data, continuous meteorological and water column observations, as well as bottom pressure measurements at data stations. The novel data used here consist of satellite data originating from the Medium Resolution Imaging Spectrometer (MERIS) onboard the ESA satellite ENVISAT with a spatial resolution of 300 m.

The observations provide high-quality signals allowing to address the temporal variability over long time periods (years). It is demonstrated that the largest velocity shears resolved by the ADCP occur in the surface mixed layer (about 1 m thick). They reveal the difference between wind and tidal currents. Furthermore, the high resolution of remote sensing data (much higher than any known resolution of earlier investigations covering the entire area of East Frisian Wadden Sea) allowed for the first time the discovery of new sediment distribution patterns. North of the barrier-islands, simulated low salinity waters originating from the tidal basins show a good (negative) correlation with

observed and simulated high sediment concentrations. The sediment regimes in the German Bight are seasonal. In winter, the sediment patterns penetrate deeply into the German Bight, whereas in summer the concentrations are lower, the gradient between tidal basins and German Bight not penetrating much north of the barrier islands. This behaviour is not only due to higher waves and stronger winds in winter, but also to the strong dependence of settling velocity on the kinematic viscosity, which changes seasonally.

The data analysed in this study enabled a detailed validation of numerical models not only at fixed locations, but also over larger areas of the Wadden Sea. Temporal variability at fixed locations is well resolved by the sediment transport model, both in phase and in amplitude. Even more promising is the agreement between spatial patterns in MERIS data and simulations, which serves as a motivation to more deeply concentrate on the practical aspects of numerical modelling and the synergy between modelling and observations in future studies.

7 Appendix

Appendix 1. Technical Characteristics of data station "WATT"

The station "WATT" (Fig. 16) is designed for a full-year operation. Its mechanical structure consists of a pole, driven to 10 m depth into the sediment, and a plat-form on top of the pole about 7 m above the mean sea level, equipped with two containers. The containers carry a second platform where a wind energy converter and solar panels are installed in order to ensure an autonomous electrical power supply. The electric system includes 750 W wind energy converter and 120 W solar panels, as well as 2500 Ah 24 V batteries and 2 kW 230 V AC gas generator. The telemetry uses a point-to-point radio link to land station on Spiekeroog Island with 2 MB/s data transfer rate. The data are further transferred the University of Oldenburg via ISDN telephone network.

Vertical access ladders and five platforms at different depths between sea surface and bottom allow safe access to the pole. Specific tubes have been installed into the pole at different water depths with a horizontal orientation along the main tidal current direction, thus leading to a continuous flow of seawater to sensors which can be attached through mounting flanges.

The station was built in Aug/Sept 2002; the first continuous measurements of meteorological and hydrographic parameters were done in October 2002. The measurements consist of temperature and salinity at 9.0, 7.5, 5.5, 3.5 and 1.5 m above sea floor. Pressure is measured at 1.5 m above sea floor. Meteorological sensors are installed on the upper platform at 14.5 m above mean low water at spring tide measuring wind direction and speed, air temperature and atmospheric pressure. Downwelling irradiance, as well as water leaving radiance is also measured.

An important component of the data station is the upward-looking Acoustic Doppler Current Profiler (operated by Senckenberg Institute, Wilhelmshaven) installed at 70 cm above the bottom. Continuous velocity measurements are performed with 20 cm vertical discretization. The data analysed in this paper are 5 min averages of the original observations.

Appendix 2. Model Description

The present work uses results of numerical simulations with the General Estuarine Transport Model (GETM) coupled with a sediment transport module (see Fig. 17). GETM is a 3-D primitive equation numerical model (Burchard

and Bolding, 2002). The governing equations in Carthesian co-ordinates read:

$$\frac{\partial u}{\partial t}+\gamma\Big(\frac{\partial(u^2)}{\partial x}+\frac{\partial(uv)}{\partial y}-fv+\frac{\partial(uw)}{\partial z}\Big)=-\frac{1}{\rho_0}\frac{\partial p}{\partial x}+\frac{\partial}{\partial z}\Big(A_V^M\frac{\partial u}{\partial z}\Big)+A_H^M\nabla^2 u \quad (1)$$

$$\frac{\partial v}{\partial t}+\gamma\Big(\frac{\partial(uv)}{\partial x}+\frac{\partial(v^2)}{\partial y}+fu+\frac{\partial(vw)}{\partial z}\Big)=-\frac{1}{\rho_0}\frac{\partial p}{\partial y}+\frac{\partial}{\partial z}\Big(A_V^M\frac{\partial v}{\partial z}\Big)+A_H^M\nabla^2 v \quad (2)$$

$$\frac{\partial u}{\partial x}+\frac{\partial v}{\partial y}+\frac{\partial w}{\partial z}=0 \quad (3)$$

$$\frac{\partial(T,S)}{\partial t}+u\frac{\partial(T,S)}{\partial x}+v\frac{\partial(T,S)}{\partial y}+w\frac{\partial(T,S)}{\partial z}=\frac{\partial}{\partial z}\left(A_V^{(T,S)}\frac{\partial(T,S)}{\partial z}\right)+A_H^{(T,S)}\nabla^2(T,S), \quad (4)$$

where u, v, and w are the velocity components with respect to the x (east), y (north), and z (upward) direction, f is the Coriolis parameter, g the acceleration due to gravity, ζ is the sea-surface height, $A_V^M(k,\varepsilon,\gamma)$ is a generalized form of the vertical eddy viscosity coefficient, $A_V^{(T,S)}$ and $A_H^{(T,S)}$ are vertical and horizontal eddy diffusivity coefficients, correspondingly, k the turbulent kinetic energy (TKE) per unit mass, and ε the eddy dissipation rate (EDR) due to viscosity. The lateral eddy viscosity/diffusivity is $A_H^M(x,y)=A_H^{(T,S)}=10\ \mathrm{m^2 s^{-1}}$.

In GETM, the process of drying and flooding is incorporated in the hydrodynamical equations through a parameter γ which equals unity in regions where a critical water depth D_{crit} is exceeded and which approaches zero when the thickness of the water column $D=H+\zeta$ tends to a minimum value D_{min}:

$$\gamma=\min\left(1,\frac{D-D_{min}}{D_{crit}-D_{min}}\right), \quad (5)$$

where H is the local depth (constant in time), taken as the bottom depth below mean sea level in the model area. Actually, the "drying corrector" reduces the influence of some terms in the momentum equations in situations of very thin fluid coverage on the tidal flats. The minimum allowable thickness D_{min} of the water column is 2 cm and the critical thickness D_{rit} is 10 cm (Burchard and Bolding, 2002, and Stanev et al., 2007b). For a water depth greater than 10 cm ($D\geq D_{rit}$) $\gamma=1$, and the full physics are included. In the range between critical and minimal thickness (between 10 and 2 cm), the model physics are gradually switched towards friction domination, i. e. by reducing the effects of horizontal advection and Coriolis acceleration in Eqs. (1) and (2) and varying the vertical eddy viscosity coefficient A_V^M according to

$$A_V^M=\nu_t+(1-\gamma)\nu_\gamma, \quad (6)$$

where $\nu_\gamma=10^{-2}\ \mathrm{m^2 s^{-2}}$ is a constant background viscosity. The eddy viscosity

ν_t is obtained from the relation

$$\nu_t = c_\mu^4 \frac{k^2}{\varepsilon}, \tag{7}$$

where $c_\mu = 0.56$ (see, e. g. Rodi 1980).

In GETM, the momentum equations (1) and (2) and the continuity equation (3) are supplemented by a pair of equations describing the time evolution of the TKE and EDR ($k - \varepsilon$ turbulence model).

$$\frac{\partial k}{\partial t} - \frac{\partial}{\partial z}\left(\frac{\nu_t}{\sigma_k}\frac{\partial k}{\partial z}\right) = P - \varepsilon \tag{8}$$

$$\frac{\partial \varepsilon}{\partial t} - \frac{\partial}{\partial z}\left(\frac{\nu_t}{\sigma_\varepsilon}\frac{\partial \varepsilon}{\partial z}\right) = \frac{\varepsilon}{k}\left(c_1 P - c_2 \varepsilon\right) \tag{9}$$

where σ_k and σ_ε are the turbulent Schmidt numbers (Rodi, 1980).

There is clear observational evidence that the velocity profiles close to the bottom in the East Frisian Wadden Sea may be adequately described by a logarithmic boundary layer (Davis and Flemming, 1991 ; Antia, 1993):

$$\frac{u}{u_*^b} = \frac{1}{\kappa} ln\left(\frac{z + z_0}{z_0}\right) \tag{10}$$

where $u_*^b = \sqrt{\frac{\tau_b}{\rho_w}}$ is the friction velocity at the sea floor, $\tau_b = \rho_w \nu_t (\partial u/\partial z)$ is the bed shear- stress, ρ_w is the water density, k is the von Karman constant, and z_0 is the bottom roughness length.

Boundary conditions for Eqs. (7) and (8) are described in detail by Burchard and Bolding (2002) and Stanev et al. (2003a) along with the parameterisations used. The parameter z_0, which gives a general representation of the bottom roughness, is taken constant over the whole area.

The sediment transport model uses a standard diffusion-advection equation for the concentration c, where settling is added on the right hand side:

$$\frac{\partial c}{\partial t} + u\frac{\partial c}{\partial x} + v\frac{\partial c}{\partial y} + w\frac{\partial c}{\partial z} = \frac{\partial}{\partial z}\left(A_V \frac{\partial c}{\partial z}\right) + \frac{\partial}{\partial z}\left(w_s c\right) \tag{11}$$

In the above equation w_s is the settling velocity of the sediment in suspension. For the cohesive sediments, which include mud particles and parts of the silt fraction, the settling velocity is concentration dependent.

In the following we present first the parameterization associated with the cohesive

sediments, to which we refer to as fine SPM ($d < 63\,\mu$m). Higher concentrations result in the formation of larger aggregates which in turn have a larger settling velocity. Experiments reveal a strong increase of the settling velocity with the sediment concentration (van Leussen, 1988), which is expressed by the formula

$$w_s = k_s c_{nd}^{m_s}, \tag{12}$$

where $c_{nd} = \frac{c}{c_{un}}$ is a non-dimensional concentration of the grain size in question, $c_{un} = 1$ kg m^{-3}, k_s and m_s are empirical constants. These are chosen to be $k_s = 0.017\,\mathrm{ms}^{-1}$ and $m_s = 1.33$ in agreement with the measurements summarized in van Leussen (1988).

The sediment flux at the sea bed

$$\left(A_V \frac{\partial c}{\partial z} + w_s c \right)_{z=-H} = E - D, \tag{13}$$

which is the bottom boundary condition of Eq. 11, is based on well-known parameterization of deposition and erosion rates D and E. The deposition rate given by Einstein and Krone (1962) is

$$D = w_s c_b \left(1 - \frac{\tau_b}{\tau_d} \right), \tag{14}$$

where c_b is the fine SPM concentration near the bottom, τ_b is the bed shear stress and τ_d is the critical shear stress for deposition.

The erosion rate is computed using the formula of Partheniades (1965):

$$E = \alpha M_e \left(\frac{\tau_b}{\tau_e} - 1 \right), \tag{15}$$

where M_e is an empirical constant giving the erosion rate at twice the critical shear stress for erosion. The parameter α specifies the fraction of the grain size in question in the bottom sediment and is 0.5 for both sediment types. The value used for M_e is $3.7 \cdot 10^{-6}$ kg m^{-2}s^{-1}.

The critical shear stress for erosion of fine SPM is set constant to $0.2\,\mathrm{Nm}^{-2}$. The critical shear stress for deposition is chosen to be equal to that for erosion.

The sediment source at the bottom is taken (as a first order approximation) to be inexhaustible for sand and fine SPM everywhere. Effects of erosion or deposition on the bottom topography are not considered in our simulations. If the water depth equals D_{min} the location is considered dry and the sediment equations are not solved any more until the water depth rises again.

The impact of wind waves on the sedimentary system in the same area is addressed earlier by Stanev et al. (2007b), where it has been demonstrated that breaking wind waves affect sediment concentrations considerably, in particular on the shallows (usually in the back barrier basins). Because the present study is focused on sediment patterns north of the barrier islands, and because winds are relatively weak for most cases addressed here, it is do not account for the effect of wind waves, assuming that model forcing is dominated by moderate winds (magnitude of 5 m/s) in the region of interest.

The sub-grid scale parameterisations are of utmost importance for the sediment transport, and the analysis of simulations by Stanev et al. (2007b) demonstrates that the general characteristics of turbulence in the bottom boundary layer are consistent with the requirements formulated by Dyer and Soulsby (1999) for correct prediction of sediment transport rates. Two of the characteristics are the logarithmic velocity profile and the parabolic-like distribution of coefficient of vertical turbulent exchange.

ACKNOWLEDGEMENTS We thank the European Space Agency ESA for providing the MERIS data within Category-1 Project No. 1359 Budget and States of the Wadden Sea Tidal Flat Water Column. G. Brink-Spalink and N. Gemein helped in numerical simulations and processing MERIS data. We are indebted to S. Dick for providing the MERIS data and data from the BSH operational model. We are very grateful to Christopher Mooers for his comments about the paper. Part of the modelling project work has also been funded by the EU-FP6 IP Project ECOOP, No. 036355

References

[1] Antia, E., Sedimentology, morphodynamics and facies association of a mesotidal barrier and island shoreface (Spiekeroog, Southern North Sea), 1993, Berichte aus dem Fachbereich Geowissenschaften der Universität Bremen, 32, 370 pp.

[2] Becker, G.A., Giese, H., Isert, K., Känig, P., Langenberg, H., Pohlmann, T., & Schrum, C., Mesoscale variability in the German Bight, 1999, Deutsche Hydrogr. Zeitung, 51, No. 2/3, 155-179.

[3] Burchard, H., & Bolding, K., GETM - a General Estuarine Transport Model, 2002, Scientific Documentation, No EUR 20253 EN, European Commission, printed in Italy, 157 pp.

[4] Davis, R.A., Flemming, B.W., Time-series study of mesoscale tidal bedforms, Martens Plate, Wadden Sea, Germany, 1991, Can. Soc. Petrol. Geol. Mem. 16, 275-282.

[5] Dick, S.K., Eckard, K., Müller-Navarra S.H., Klein, H., & Komo, H., The operational circulation model of BSH (BSHcmod) - Model description and

validation, 2001 Berichte des Bundesamtes für Seeschifffahrt und Hydrographie (BSH), 29, 49pp.

[6] Doerfer, R., Sorensen, K., & Aiken, J., MERIS potential for coastal zone applications, 1999, International Journal of Remote Sensing, 20(9), 1809-1818.

[7] Doxaran, D., Lavender, S.J., & Froidefond, J.-M., Mapping tidal and seasonal movements of the maximum turbidity zone in estuarine waters from remotely sensed (SPOT, LANDSAT) data, 2004, A semi-empirical approach. EARSeL eProceedings, 3(1), 54-68.

[8] Droppert, L.J., Cattle, H., Stel, J.H., & Behrens, H.W.A., (eds.), The NOOS Plan: North West Shelf Operational Oceanographic System, 2002-2006, 2000 EuroGOOS Publication No. 18, Southampton Oceanography Centre, Southampton. ISBN 0-904175-46-4.

[9] Dyer, K.R., & Soulsby, R.L., Sand transport on the continental shelf, 1988, Annual Review of Fluid Mechanics 20: 295-324.

[10] Einstein, H.A., & Krone, R.B., Experiments to determine modes of cohesive sediment transport in salt water, 1962 J. Geophys. Res,, 67, 1451-1461.

[11] European Space Agency ESA,2004. MERIS Product Handbook, Chapter 3.1.

[12] Flemming, B.W., Factors affecting the shape of particle frequency distribution and associated textural parameters, 2004, In: From particle size to sediment dynamics, edited by B W Flemming, 53-58.

[13] Friedrichs, C.T., & Madsen, O.S., Nonlinear diffusion of the tidal signal in frictionally dominated embayments, 1992, J. Geophys. Res., 97, 5637?5650.

[14] Gayer, G, & Dick, S., Numerical modeling of suspended matter transport in the North Sea, 2006, Ocean dynamics 56(1), 62-77.

[15] Gemein, N., Stanev, E.V., Brink-Spalink, G., Wolff, J.O., & Reuter, R., Patterns of suspended matter in the East Frisian Wadden Sea: Comparison of numerical simulations with MERIS observations, 2006, EARSel eProceedings, 5(2), 180-198.

[16] Janssen, F., Schrum, C., & Backhaus, J., A Climatological Data Set of Temperature and Salinity for the Baltic Sea and the North Sea, 1999, Dt. hydrogr. Z., Supp. 9.

[17] Jördel, O., Flemming, B.W., & Bartholom, A., Flocculation, floc-breakup and grain-size composition of suspended sediments in tidal waters of the southern North Sea, 2004, in: Flemming, B.W., Hartmann, D., Delafontaine, M.T. (eds.): From Particle Size to Sediment Dynamics. Intern. Workshop, 15-18 April 2004, Hanse Institute for Advanced Study, Delmenhorst, Germany. Research Center Terramare Reports, No. 13, 86-89.

[18] Krögel, F., & Flemming, B.W., Evidence for temperature adjusted sediment distribution in the backbarrier tidal flats of the East Frisian Wadden Sea (southern North Sea), 1998, In: Alexander C.R., Davis R.A., Henry V.J. (eds) Tidalites: Processes and products. SEPM Spec Publ, 61, 31-41.

[19] Lehner, S.,Anders, I., & Gayer, G., High resolution maps ofsuspended particulate matter concentration in the German Bight, 2004, EARSeL eProceedings, 3(1), 118-126.

[20] van Leussen, W., Aggregation of particles, settling velocity of mud flocks, 1988, In: Dronkers J and van Leussen W (eds) Physical Processes in Estuaries, pp 347-404.

[21] Münchow, A., Tidal currents in a topographically complex channel, 1998, Cont. Shelf Res., 18, 561- 584.

[22] Pleskaschevski, A., Gayer, G. , Horstmann, J., & Rosenthal, W., Synergy of Satellite Remote Sensing and Numerical Modeling for Monitoring of Suspended Particulate Matter, 2005, Ocean Dynamics, DOI $10.1007/s10236-004-0101-z$, Vol. 55(1), pp. 2-9.

[23] Puls, W., & Sündermann, J., Simulation of suspended sediment dispersion in the North Sea, 1990, in: R.T. Cheng (ed.), Coastal and estuarine studies, 38, Residual currents and long-term transport, Springer, New York.

[24] Reuter, R., Meeresdaten rund um die Uhr: die Station im Watt, 2005, EINBLICKE: Forschungsmagazin der Universitt Oldenburg, 41, 6-8.

[25] Rodi, W., Turbulence models and their application in hydraulics, 1980, Rep International Association for Hydraulic Research (Delft, The Netherlands) 104 pp.

[26] Santamarina Cuneo, P., & Flemming B., Quantifying the concentration and flux of suspended particulate matter through a tidal inlet of the East Frisian Wadden Sea by acoustic Doppler current profiling, 2000, in: Flemming, B.W., Delafontaine, M.T., Liebezeit, G. (Eds.) Muddy Coast Dynamics and Resource Management, Elsevier Science, Amsterdam, The Netherlands, pp 39-52.

[27] Sarangi, R.K., Chauhan, P., & Nayak, S.R., Phytoplankton bloom monitoring in the offshore water of Northern Arabian Sea using IRS-P4 OCM Satellite data, 2001, Indian Journal of Marine Sciences, 30, 214-221.

[28] Schubert, M., Blender, R., Fraedrich, K., Lunkeit, F., Pertwitz, J., North Atlantic cyclones in CO2-induced warm climate simulations: frequency, intensity and tracks, 1998, Climate Dynamics 14, 827-837.

[29] Stanev, E.V., Flöser, G., & Wolff, J.-O., Dynamical control on water exchanges between tidal basins and the open ocean, 2003a, A Case Study for the East Frisian Wadden Sea. Ocean Dynamics, 53, 146-165.

[30] Stanev, E.V., Wolff, J.-O., Burchard, H., Bolding, K., & Flöser, G., On the Circulation in the East Frisian Wadden Sea: Numerical modeling and data analysis, 2003b, Ocean Dynamics, 53, 27-51.

[31] Stanev, E.V., Brink-Spalink, G., & Wolff, J.-O., Control of sediment dynamics by transport and turbulence. A case study for the East Frisian Wadden Sea, 2007a, J Geoph Res (in press)

[32] Stanev, E., Flemming, B., Bartholomae, A., Staneva, J., & Wolff, J.-O., Vertical circulation in shallow tidal inlets and back barrier basins. Cont, 2007b, Shelf Res. doi:10.1016 csr.2006.11.019.

[33] Staneva, J., Bolding, K., & Stips, A., A nested grid model for studying the German Bight circulation, 2007, Ocean Dynamics, (in preparation)

[34] Valle-Levinson, A, & Lwiza, K.M.M., Effects of channels and shoals on the exchange between the lower Chesapeake Bay and the adjacent ocean, 1995, J.Geophys.Res., 100(C9), 18, 551-18, 563.

8 Figures

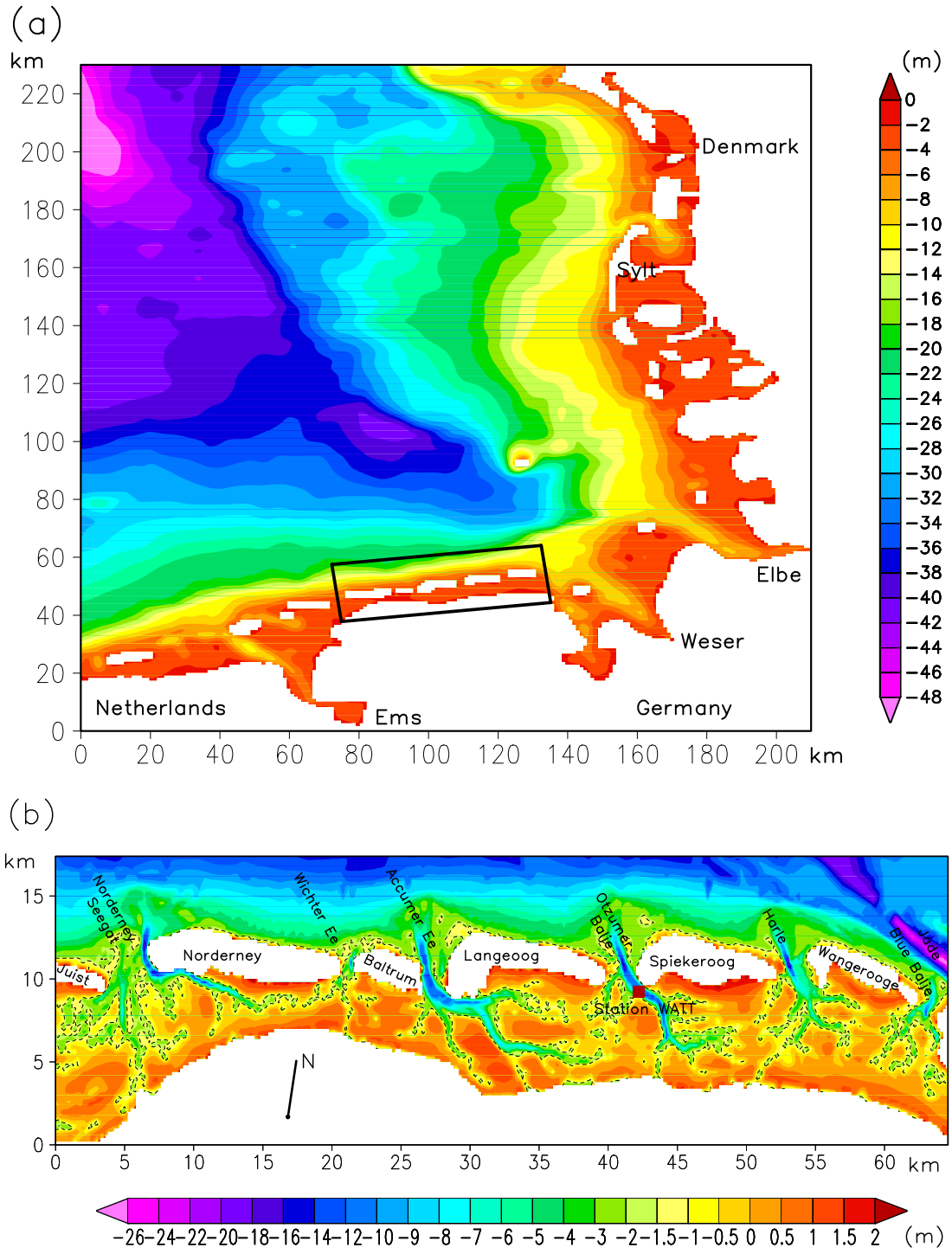

Fig. 1. Topography of the (a) German Bight and (b) Wadden Sea. The arrow in the lower panel giving the direction to the North demonstrates that the model area in the Wadden Sea is rotated, which is done in order to reduce the size of the model grid. The -1.5 m isobath plotted in the Wadden Sea map contours approximately the dry area under low water.

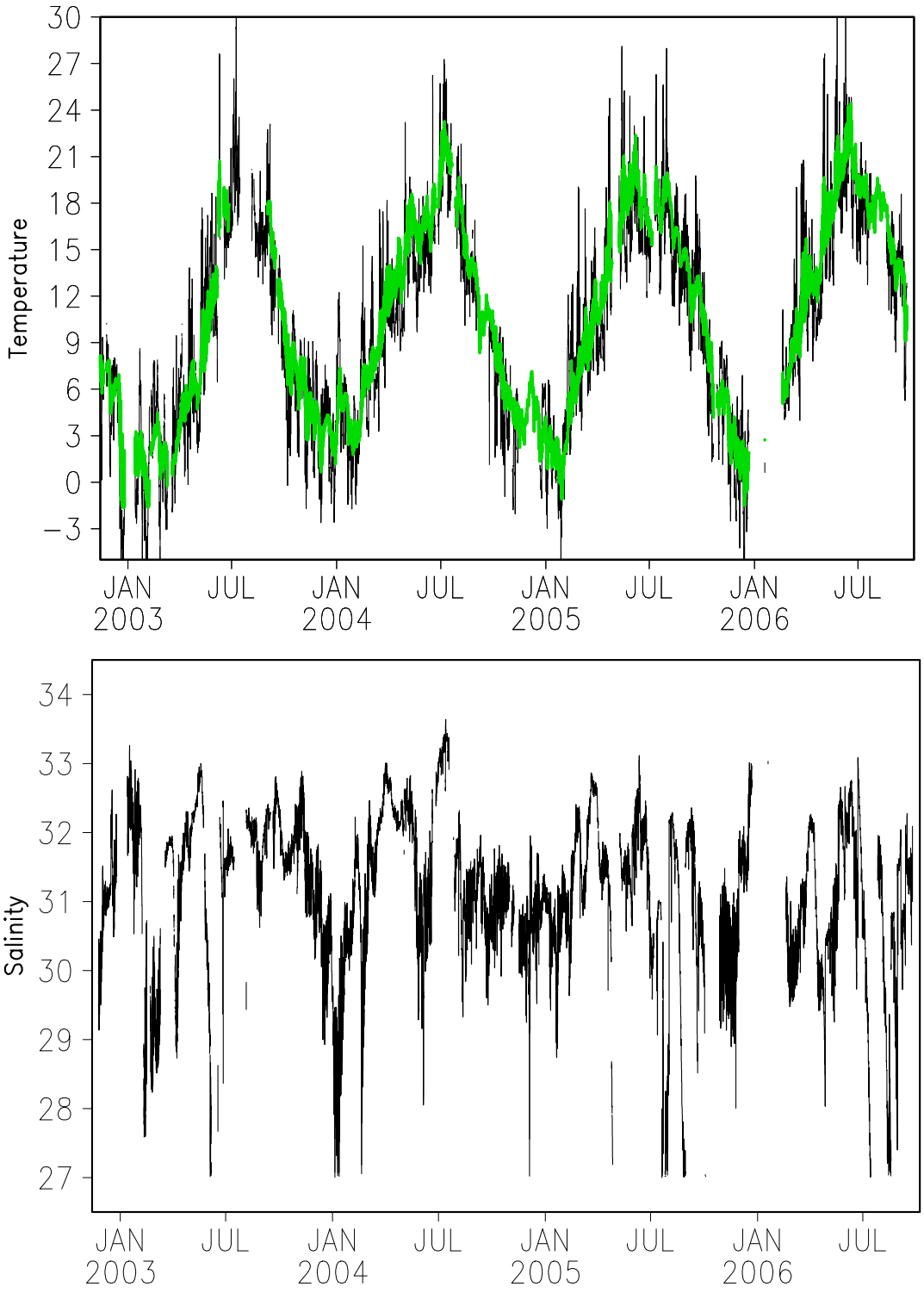

Fig. 2. Observations at the WATT data station. (a) Air (black line) and sea surface (green line) temperature (deg. C), (b) surface salinity (psu).

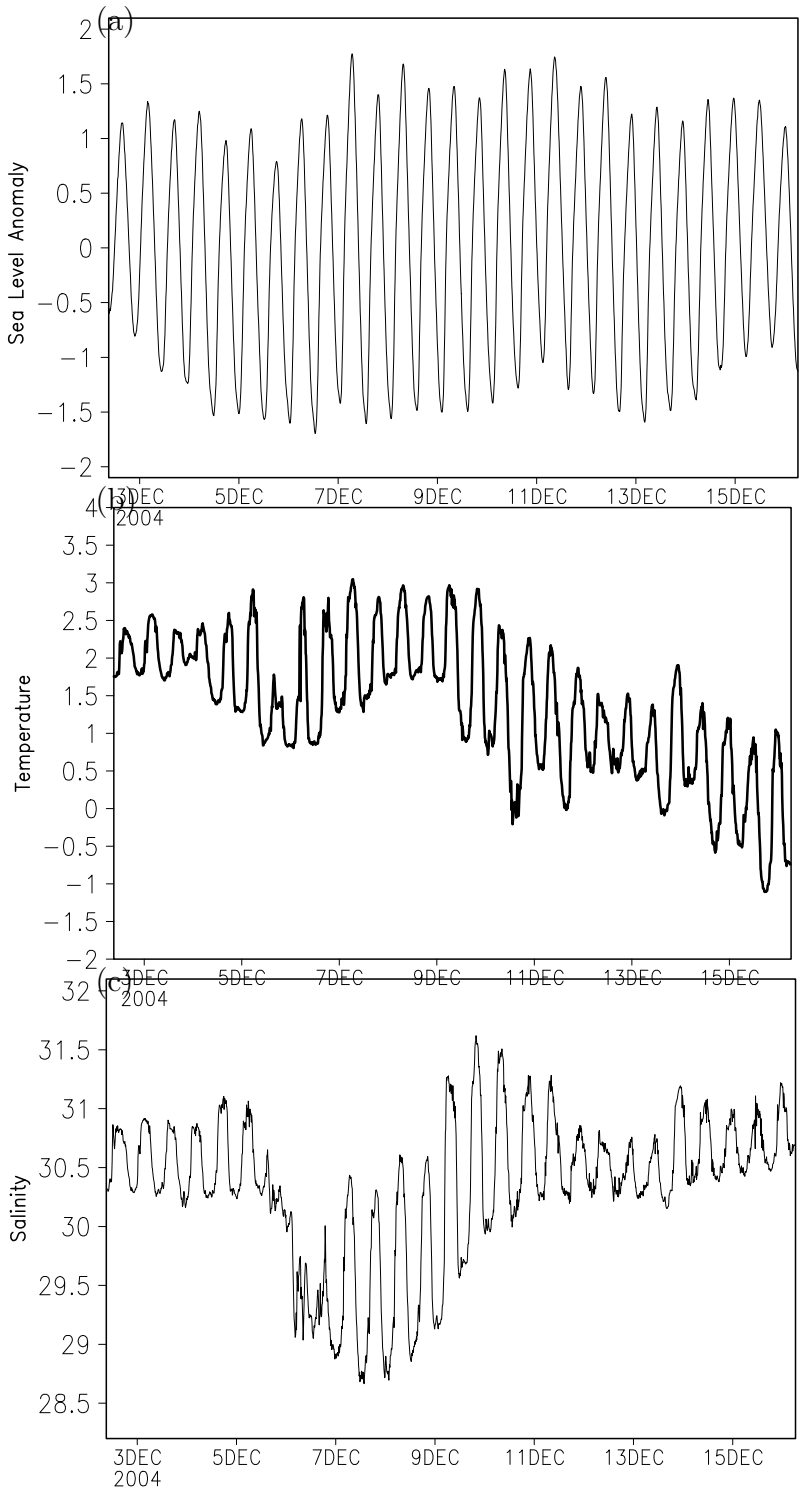

Fig. 3. Observations at the WATT data station as in Fig. 2 but zoomed for the period from 02.12.2004 to 16.12.2004 to demonstrate tidally and man-induced variability. (a) Sea level anomaly (meters), (b) surface temperature (deg. C), (c) surface salinity (psu) including an event of fresh water release from a coastal lake.

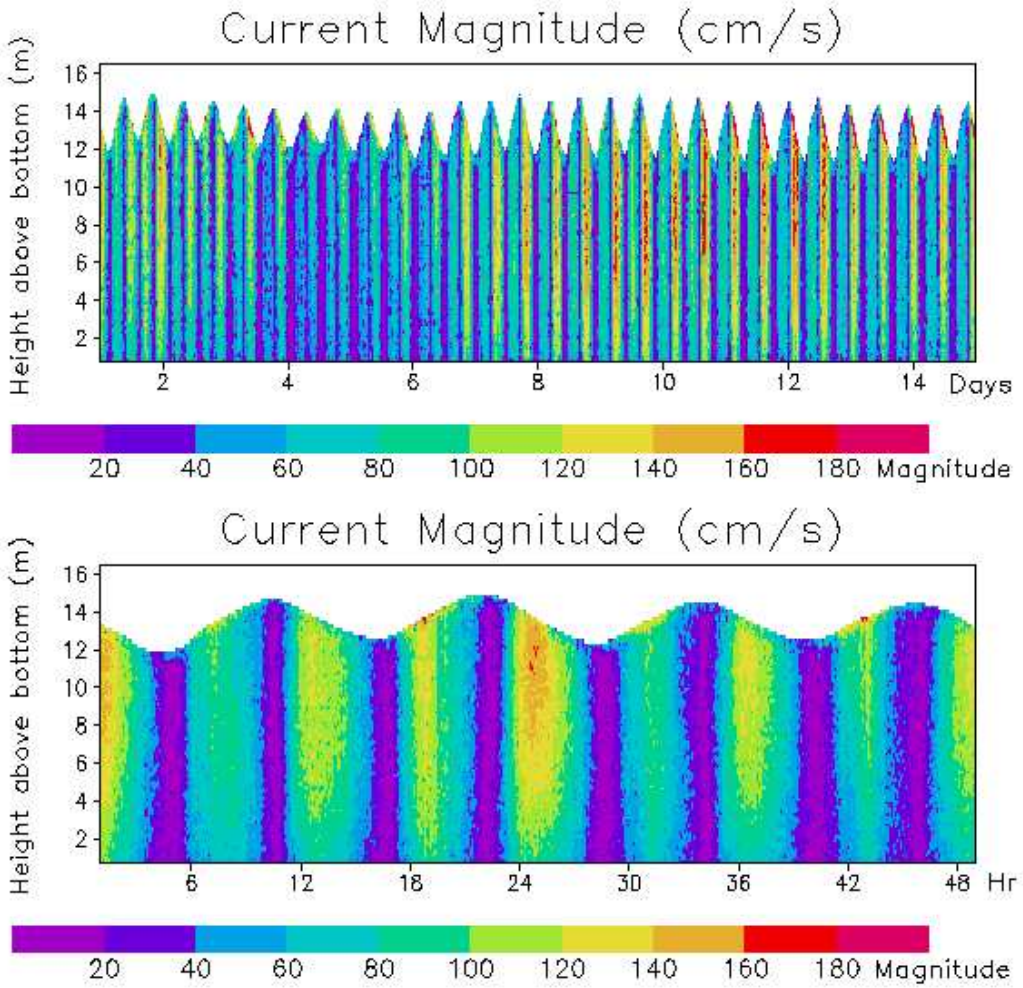

Fig. 4. ADCP data. (Upper panel) Current speed during one spring and one neap period starting from 16.03.2005, (bottom panel) current speed during four spring periods only.

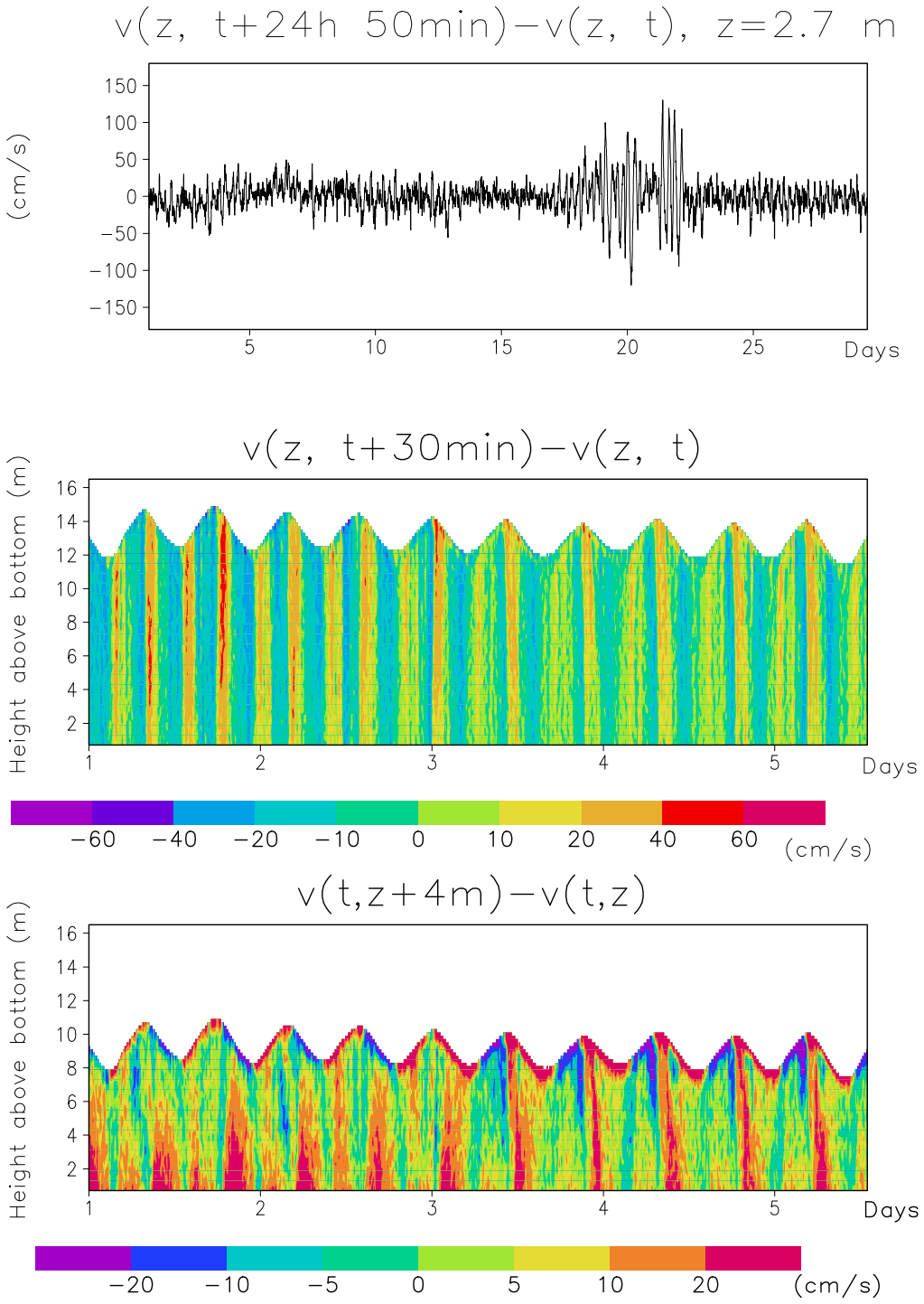

Fig. 5. ADCP data. (Upper panel) Time-lagged difference between velocity magnitude at 2.7 m above the bottom (T=24 h 50 min), (middle panel) time lag difference between velocity magnitude (T=30 min) versus depth, (bottom panel) velocity difference between depths 4 m apart one from another.

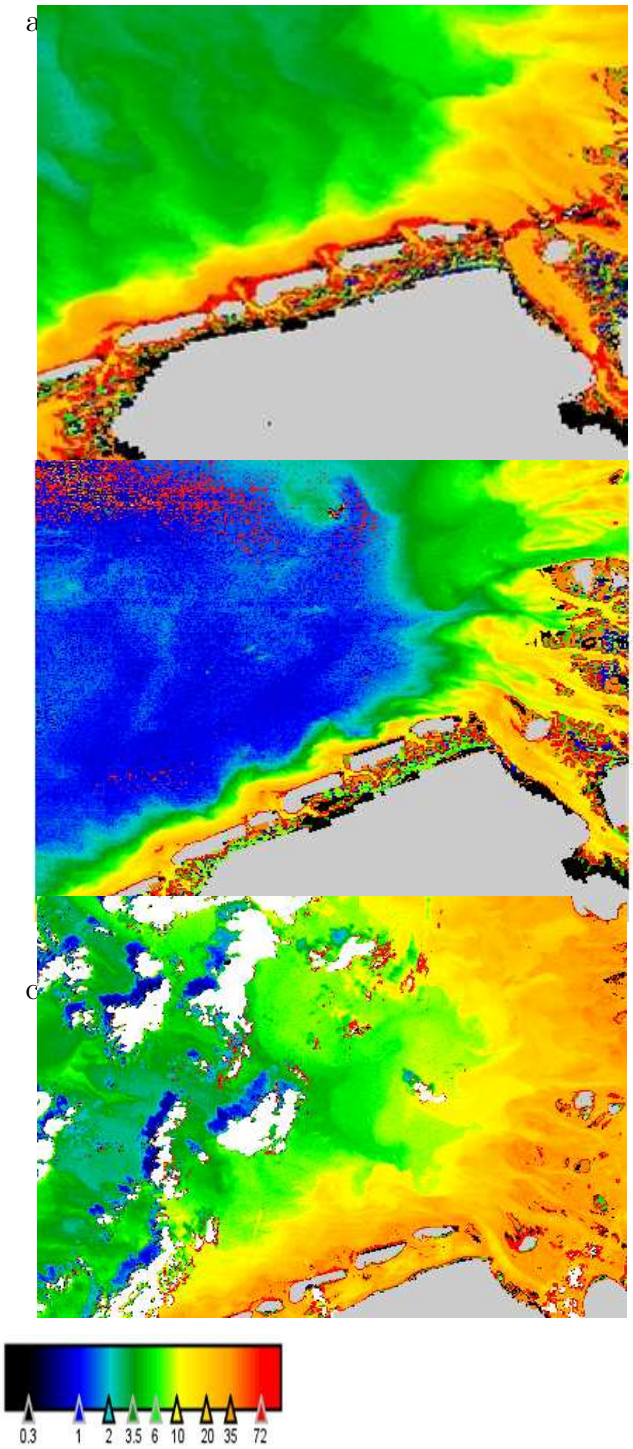

Fig. 6. MERIS derived surface images of SPM concentration (mg/l). (a) 29 March 2004, low water, 6.3 m/s northeastward wind during the last 12 hours before the image was taken, (b) 9 September 2004, 1.5 hours before low water, 5.5 m/s westward wind during the last 12 hours before the image was taken, and (c) 19 February 2005, 3 hours after high water, 5.2 m/s northeastward wind during the last 12 hours before the image was taken, with peak speed of about 10 m/s. White areas are clouds, the blue parts next to them are their shadows, the dry areas are in grey.

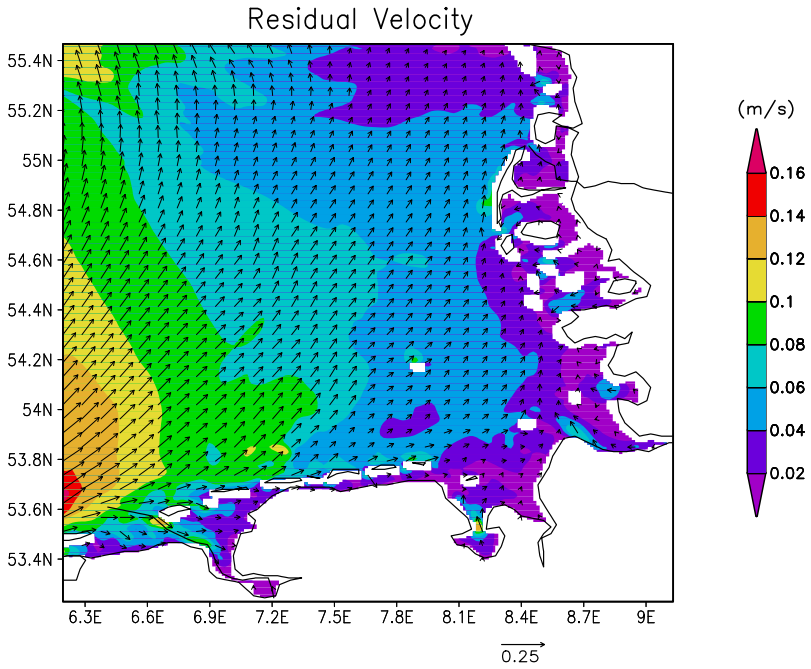

Fig. 7. Residual circulation of the German Bight Model for 2000-2005.

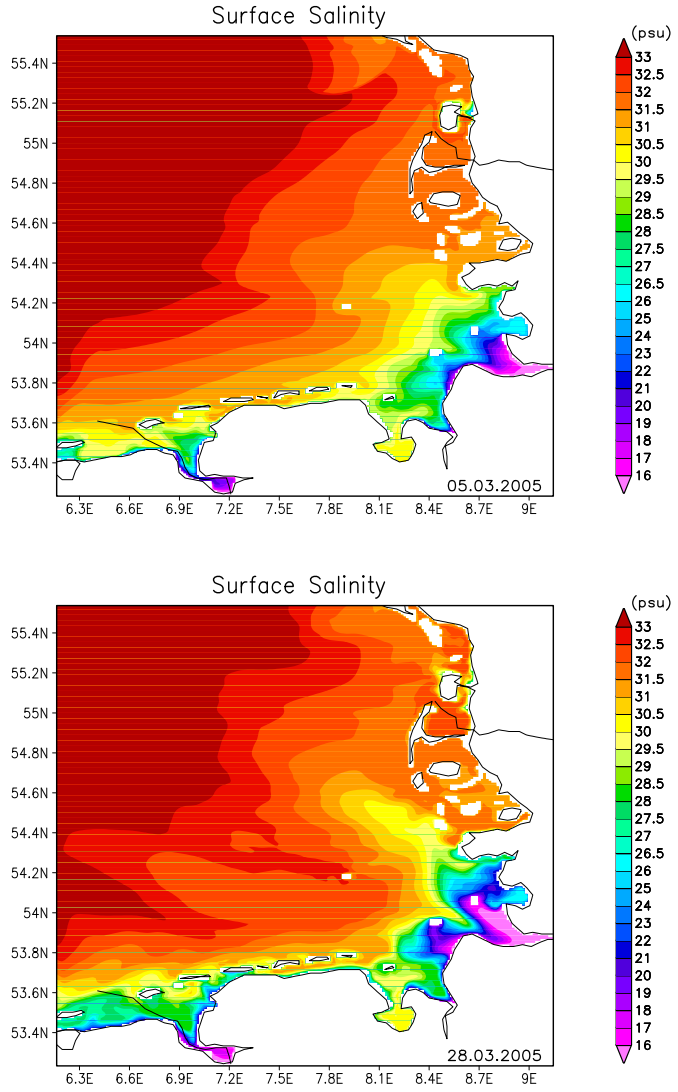

Fig. 8. Surface salinity (psu) in the German Bight. Upper panel at 05.03.2005; bottom panel at 28.03.2005.

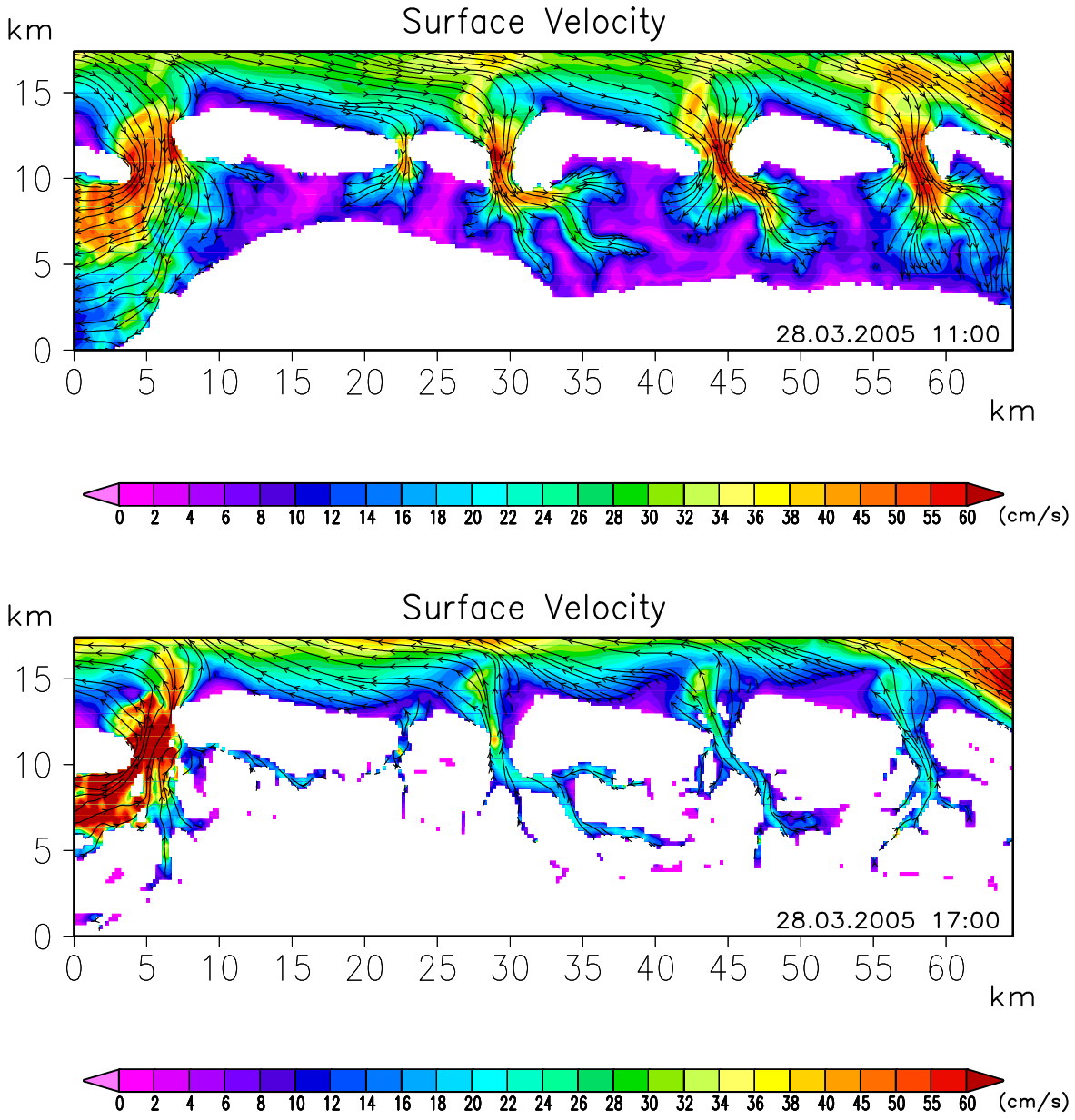

Fig. 9. Circulation in the Wadden Sea during (upper panel) hight water and (bottom panel) low water.

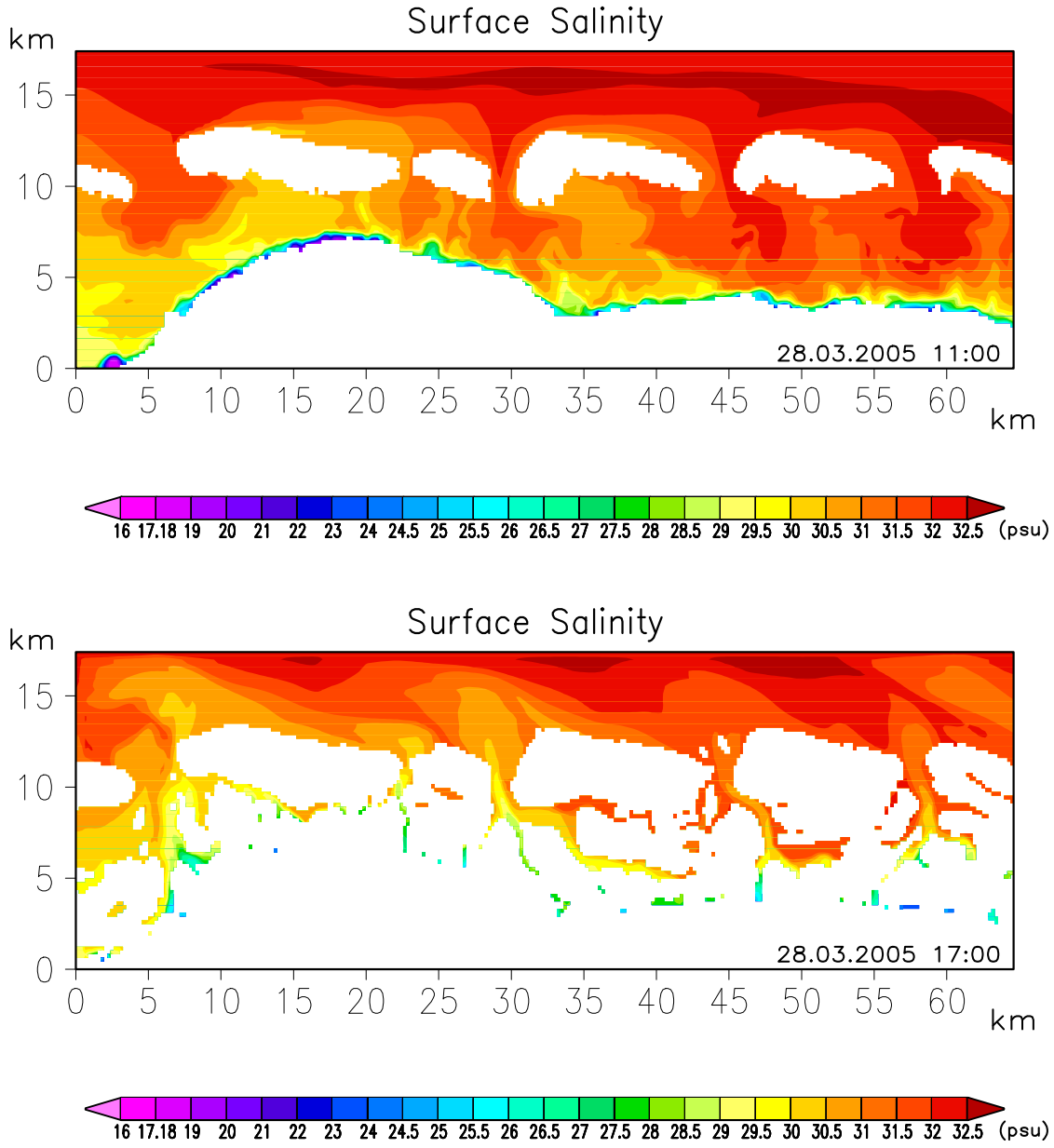

Fig. 10. Salinity in the Wadden Sea during 28.03.2005 at: (upper panel) high water, and (bottom panel) low water.

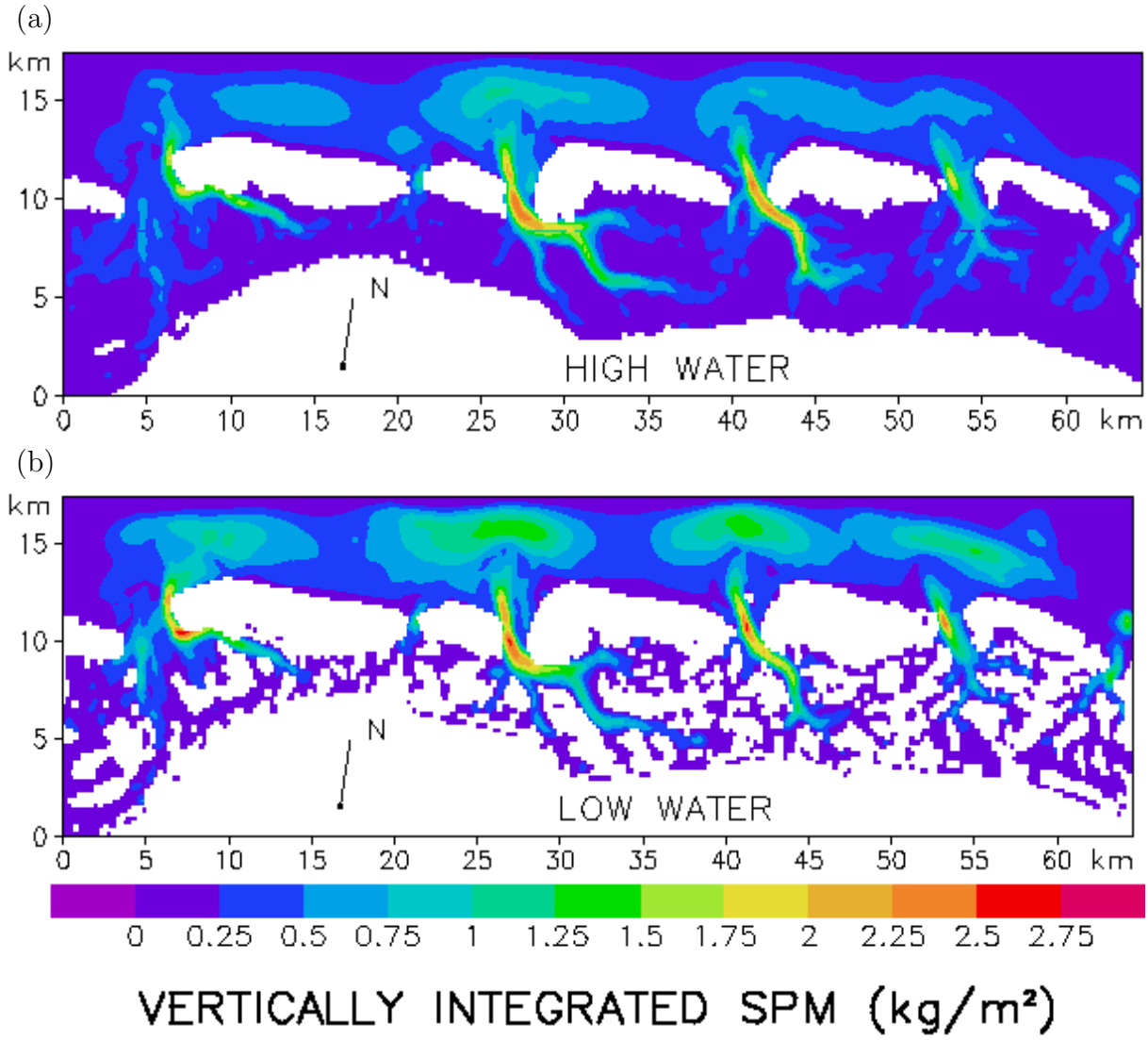

Fig. 11. Vertically integrated SPM surface concentrations during 28.03.2005. (a) High water, (b) low water. The fine SPM concentrations during high water are only half as large as during flood and ebb. The concentrations during low water reveal maxima north of the barrier islands. These large concentrations are due to the fact that during ebb the waters in the channels (and north of them) are replaced by relatively sediment-rich water from the tidal flats.

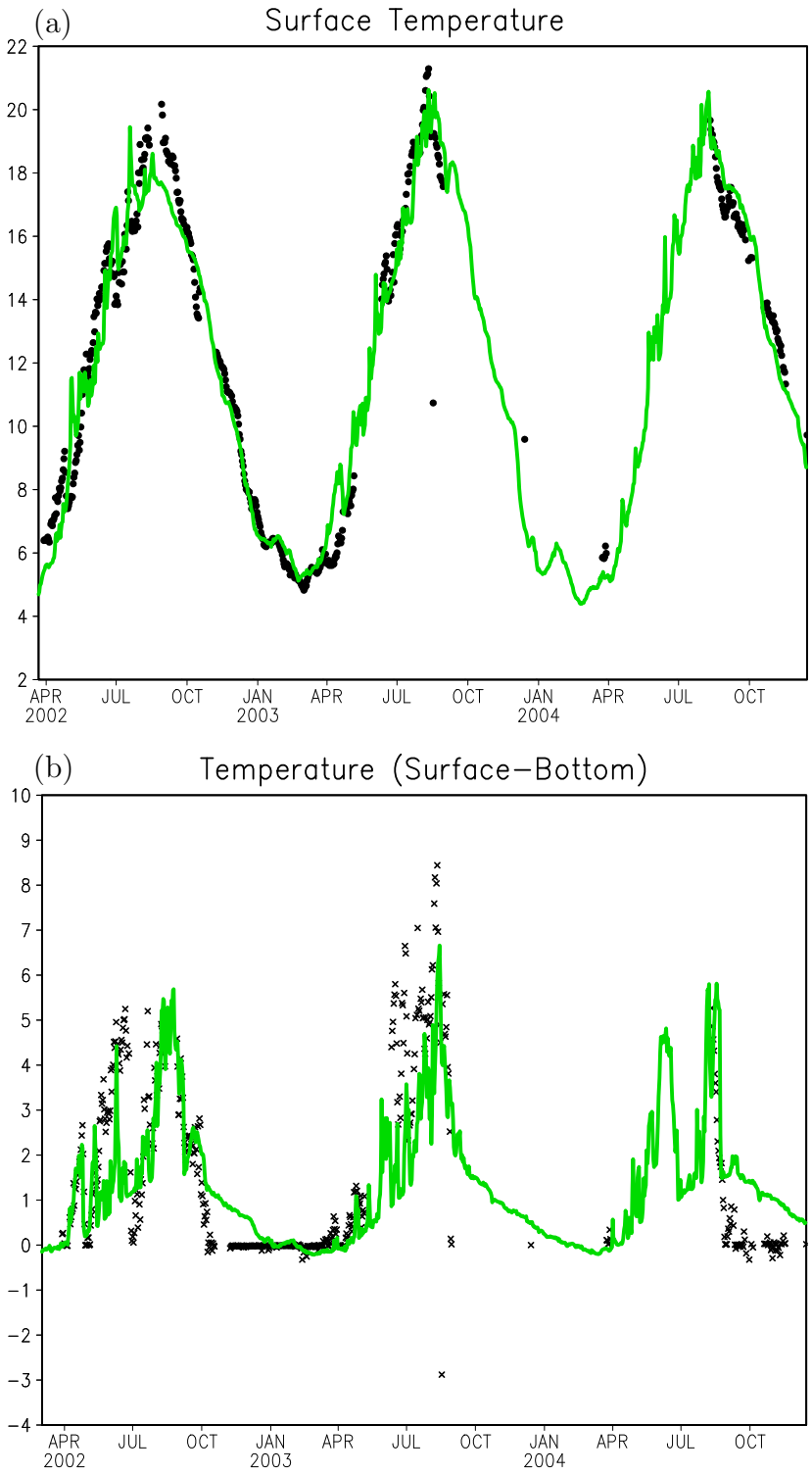

Fig. 12. Comparison of simulated and observed temperature at 54° 10′ N, 7° 27′ E (location in the German Bight MARNET Data Station). (a) Sea Surface Temperature (SST, deg. C), (b) difference between surface and bottom temperature (deg. C), green line-simulatons, black symbols-MARNET observations.

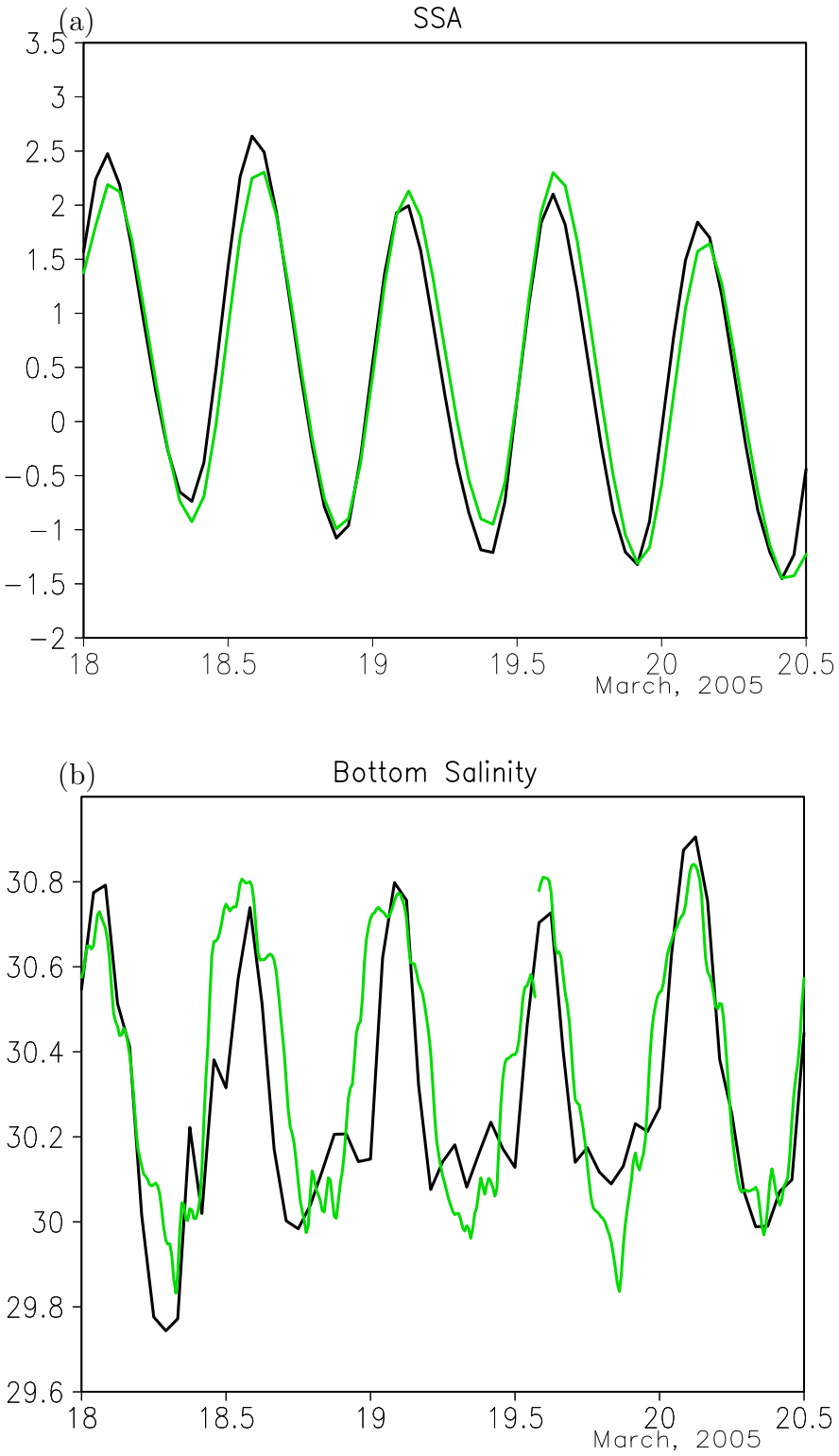

Fig. 13. Comparison at the WATT data station: green line-WATT station observations, black line-simulations plotted at the location of the station. (a) Sea surface anomaly (meters), (b) bottom salinity (psu).

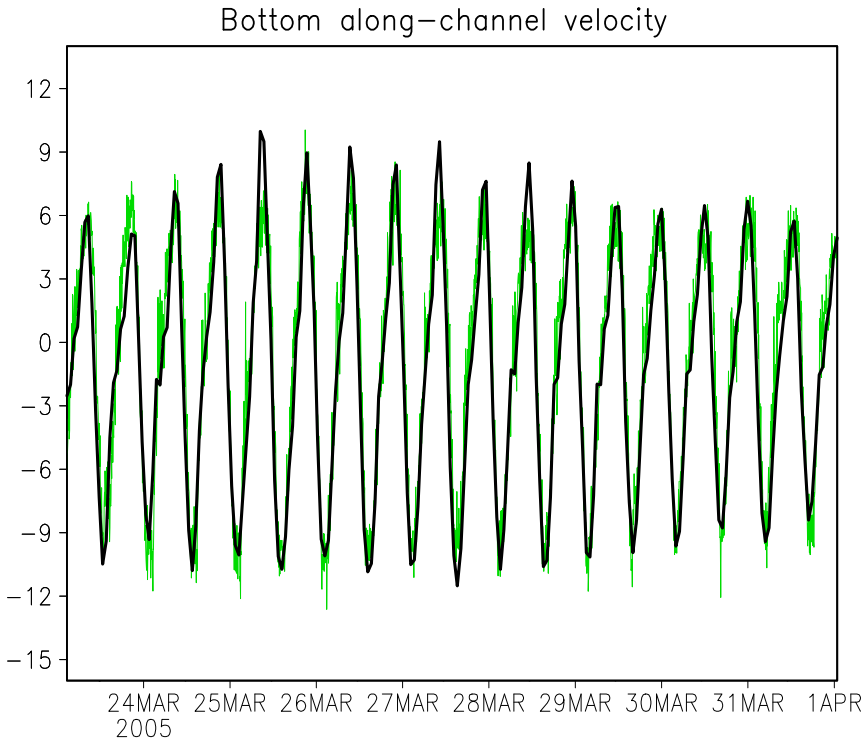

Fig. 14. Comparison at the WATT data station: green line - WATT station observations, black line - simulations plotted at the station location. Along channel velocity (cm/s, positive sign is northward directed to the German Bight).

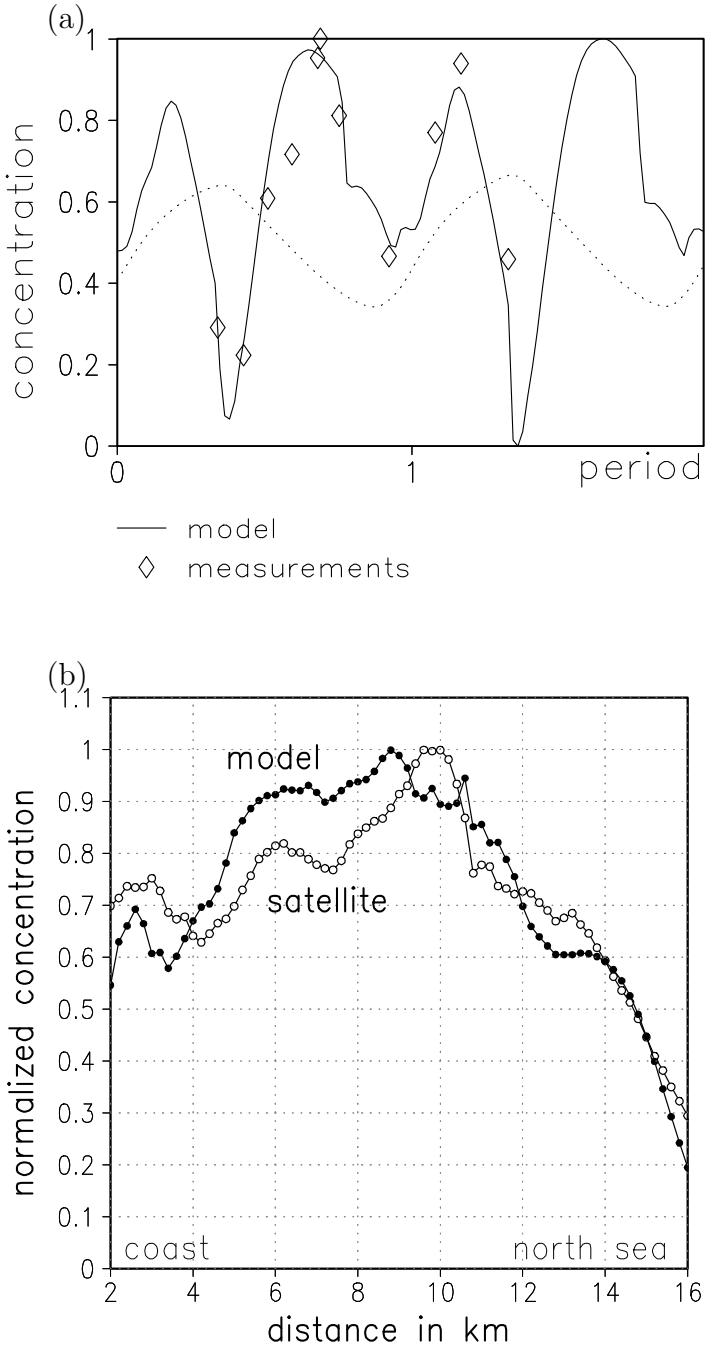

Fig. 15. Validation of the sediment transport model. (a) Normalized to absolute maximum concentration of fine SPM from observations (diamonds) and numerical simulations (1 m above the bottom, solid line). The dotted line represents the tidal oscillations of sea level. (b) Zonal-mean SPM concentrations (normalised with respect to the maximum) from simulations and observations.

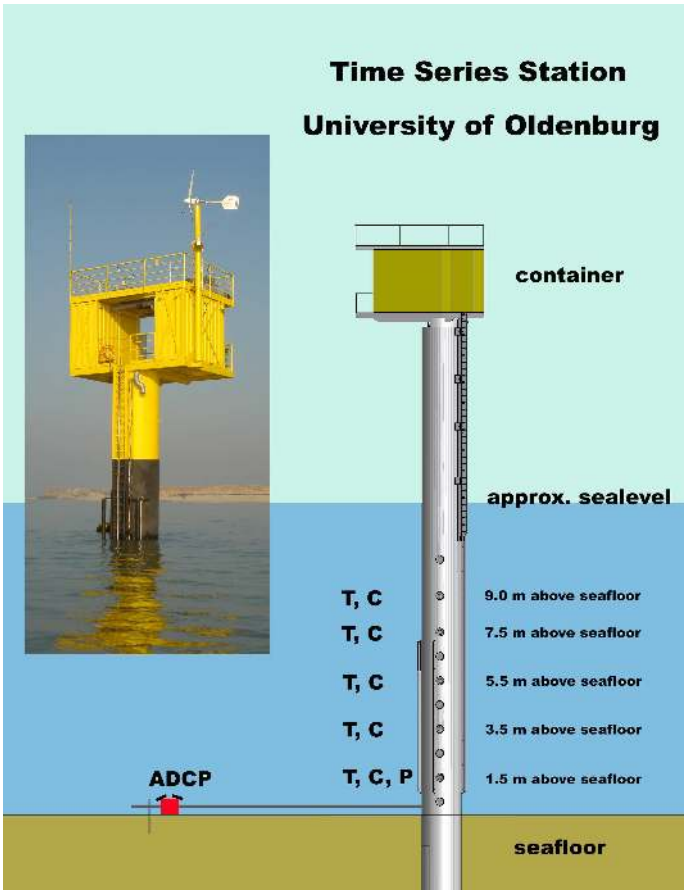

Fig. 16. Data station WATT. Left - photo of the station, right - scheme with water depths.

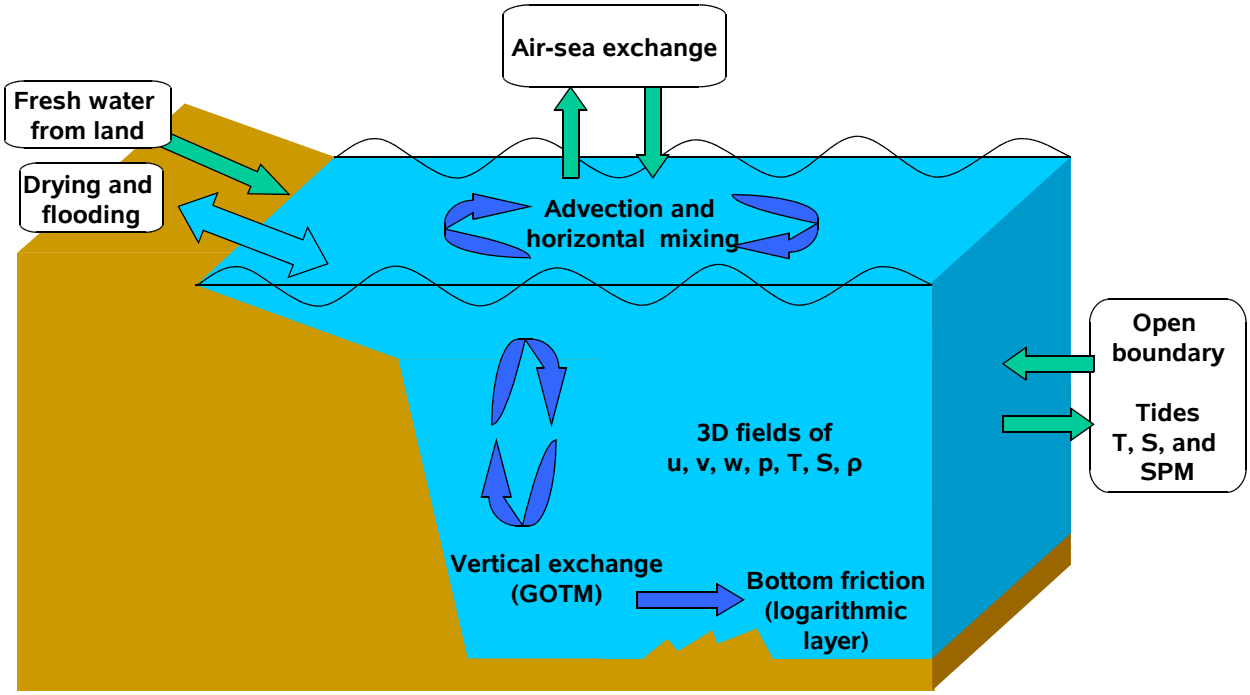

Fig. 17. Schematic presentation of the model.